

Diagnosics of SS433 with the RXTE

Filippova E., Revnitsev M.

*Space Research Institute, Russian Academy of Sciences, Profsoyuznaya
84/32, 117997 Moscow, Russia*

Fabrika S.

*Special Astrophysical Observatory, Nizhnij Arkhyz,
Karachaevo-Cherkesiya, 369167, Russia*

Postnov K., Seifina E.

Sternberg Astronomical Institute, 119992, Moscow, Russia

Abstract. We present analysis of extensive monitoring of SS433 by the RXTE observatory collected over the period 1996-2005. The difference between energy spectra taken at different precessional and orbital phases shows the presence of a strong photoabsorption near the optical star, probably due to its powerful dense wind. Assuming that a precessing accretion disk is thick, we recover the temperature profile in the X-ray emitting jet that best fits the observed precessional variations of the X-ray emission temperature. The hottest visible part of the X-ray jet is located at a distance of $l_0/a \sim 0.06 - 0.09$, or $\sim 2 - 3 \times 10^{11}$ cm from the central compact object and has a temperature of about $T_{\max} \sim 30$ keV. We discovered appreciable orbital X-ray eclipses at the “crossover” precessional phases (jets are in the plane of the sky, disk is edge-on) which put a lower limit on the size of the optical component $R/a \gtrsim 0.5$ and an upper limit on a mass ratio of binary companions $q = M_x/M_{\text{opt}} \lesssim 0.3 - 0.35$. The size of the eclipsing region can be larger than secondary’s Roche lobe because of substantial photoabsorption by dense stellar wind. This must be taken into account when evaluating the mass ratio from analysis of X-ray eclipses.

1. Introduction

SS 433 is a binary system which is thought to consist of a compact object (probably a black hole) and optical star filling its Roche lobe.

There is a supercritical accretion rate in the system (Fabrika 2004), which leads to formation of the geometrically thick accretion disk around compact object and two oppositely directed highly collimated jets.

The main contribution to the observed X-ray emission from the system comes from the optically thin multitemperature plasma in the jets via bremsstrahlung mechanism.

The X-ray emission from SS433 is subjected to systematic variations due to the thick accretion disk precession ($P_{\text{prec}} = 162.375$ days), nutation ($P_{\text{nut}} = 6.2877$ days) and orbital ($P_{\text{orb}} = 13.08211$ days) motion in the binary system (Fabrika 2004).

2. The inner jet tomography by orbital and precessional eclipses

Eclipses by the thick accretion disk and optical star result in obscuring the innermost the hottest parts of the jets from the observer which leads to the drop of the maximum temperature of the registered X-ray emission (Fig.1).

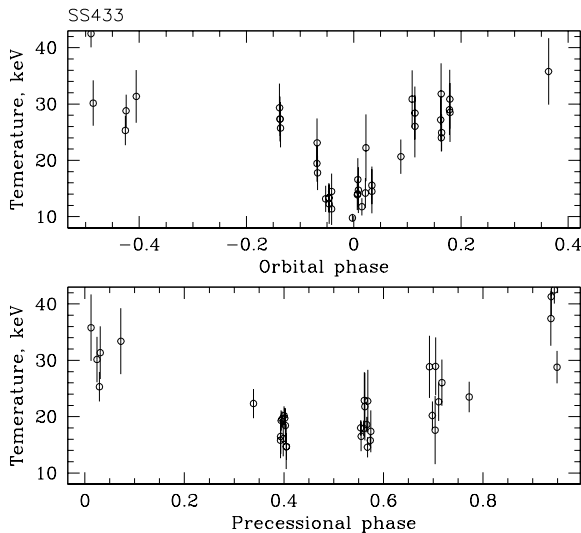


Figure 1. The temperature of optically thin thermal plasma emission observed from SS433 as a function of orbital and precessional phases. For the plot in the bottom panel only off-eclipse data were selected.

In order to find the spectral contribution from the innermost (the hottest) regions of the jet we examine differences between spectra taken during eclipses and off eclipses.

The result is presented in the Fig.2. A strong photoabsorption is observed near the orbital eclipse (the left panel of Fig.2). The best-fit value of the absorption column density in this spectrum is $N_{\text{H}} = (12.5 \pm 1.5) \times 10^{22} \text{ cm}^{-2}$, much higher than the conventional value.

The spectrum of the hottest (innermost) part of the jet as derived from precessional variations off the primary eclipse (the right panel of Fig.2) also suggests some photoabsorption, but of considerably smaller value – here the best-fit absorbing column density is $N_{\text{H}} = (4.5 \pm 1.5) \times 10^{22} \text{ cm}^{-2}$.

So our investigation shows the presence of the absorbing material in the system. Its density is much higher near the optical star. The ordinary of this

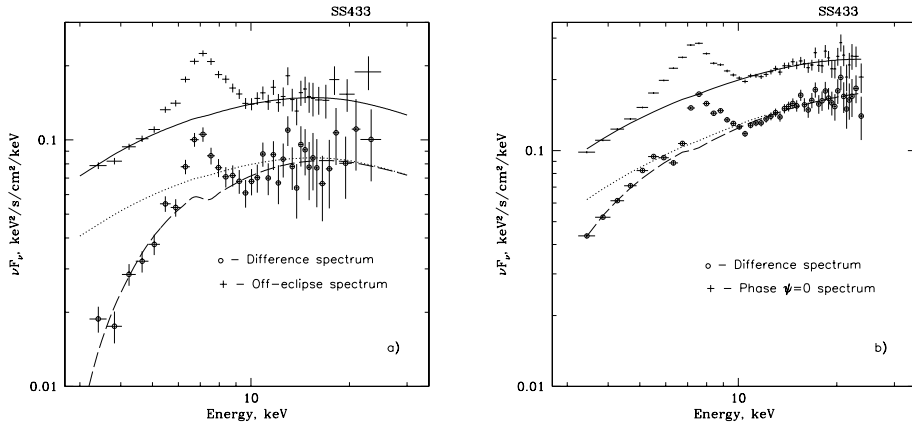


Figure 2. a) The X-ray spectrum of SS433 immediately after the eclipse (the orbital phase $\phi = 0.114$, crosses) and difference between this spectrum and that at $\phi = 0.021$. b) The X-ray spectrum of SS433 at precessional phase $\psi \sim 0$ and difference between this spectrum and that at $\psi \sim 0.4$. Solid curves show best-fit thermal bremsstrahlung model with photoabsorption. Dotted curves show best-fit bremsstrahlung models with a nominal photoabsorption column density of $N_H = 10^{22} \text{ cm}^{-2}$.

material can appear from powerful winds from the optical supergiant star and super-Eddington accretion disk.

In order to estimate the possible increase of the star radius due to the dense stellar wind we take parameters of the wind (its mass loss rate and velocity distribution) from the work of Achmad et al. (1997). In the case of the plasma with solar abundance it becomes almost opaque for X-rays when $N_H = 10^{24} \text{ cm}^{-2}$. Our estimations show that maximal value of the A supergiant mass loss rate $\dot{M} = 8 \times 10^{-7} - 10^{-6} M_\odot/\text{yr}$ can increase the size of the star up to 20 %.

3. Jet eclipses by the thick disk

We describe jets in SS433 as conical plasma flows with constant velocity $v_j = 0.26 c$ along the jet axis and constant half-opening angle $\theta = 0.61^\circ$ (Marshall et al. 2002). Radius of the jet cross section is $r = r_b + \theta l$, where r_b is the radius of the jet near the compact object ¹, l is the distance from the compact object along jet axis.

We assume that the dominant cooling process of the jet is adiabatic cooling.

So the plasma temperature T changes with distance from the compact object l as: $T/T_0 = (1 + \theta(l - l_0)/r_0)^{-4/3}$, where T_0 is the plasma temperature and

¹This analytical description does not mean that the jet should start near the compact object.

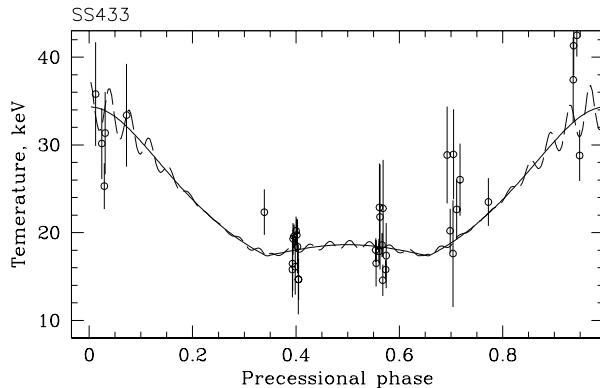


Figure 3. The plasma temperature as a function of the precessional phase. The solid curve shows the best-fit model. The dashed curve shows the same model but with nodding motion of thick accretion disk included.

r_0 is the jet cross section radius at some distance l_0 from the central source (see also Koval' & Shakura 1989).

For disk radius we adopted the disk truncation radius given by Paczynski (1977).

Comparison of the highest visible temperature profiles derived above with observational data enables us to find the model parameters (the best-fit model is shown in Fig.3). The best-fit parameters of our model referred to the distance from the black hole $l_0/a = 0.06 - 0.09$ (depending on the assumed value of q) are: the highest temperature of the jet $T_0 = 30 \pm 2$ keV, the radius of the jet $r_0/a = (1 - 1.6) \times 10^{-2}$.

4. Eclipses by the optical companion

In Fig.4(left panel) we present the profile of the maximum X-ray temperature measured in the orbital eclipse near precessional phases $\psi \sim 0.33, 0.66$. The orbital X-ray eclipse is clearly visible and shows an appreciable depth. The ratio of the maximum jet temperature derived from off-eclipse observations to that of the eclipsed jet is $\sim 1.9 \pm 0.2$. Dashed lines in the figure show examples of eclipsing profiles obtained in our model. They are not symmetric due to the different jet inclination with respect to the binary orbital plane at this phases.

The ratio of the maximum jet temperatures in the eclipse and off the eclipse is plotted in Fig.4 (right panel) as a function of the binary mass ratio q . The solid curve shows the ratio obtained under the assumption that the size of the star equals to the volume averaged radius of the Roche lobe.

We have shown in Section 2 that the size of the eclipsing region might be large then the Roche lobe of the optical star. The innermost parts of dense stellar wind also can absorb X-rays thus increasing the duration and depth of the X-ray eclipse. So in Fig. 4 (right panel) we also plot by the dotted and

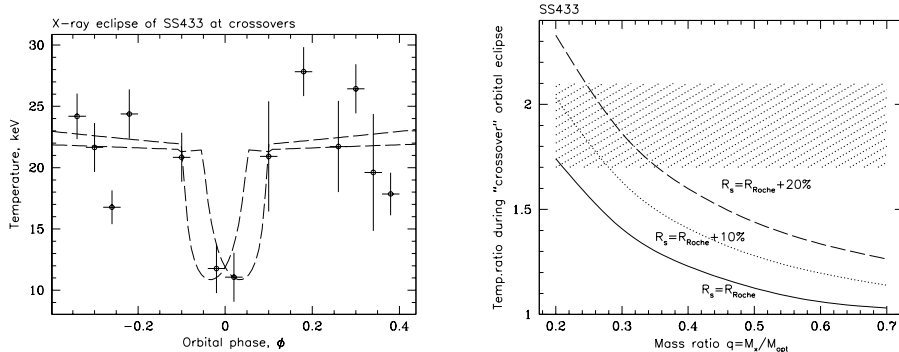


Figure 4. Left panel: orbital X-ray eclipse observed at the precessional phases $\psi \sim 0.33, 0.66$. Right panel: the ratio of the maximum visible jet temperatures during the orbital eclipse at these precessional phases as a function of the mass ratio q . The hatched area shows the observational constraints.

dashed curves the model ratio of maximum jet temperatures in- and out- of the eclipse assuming the star radius to be $R = 1.1R_{Roche}$ and $R = 1.2R_{Roche}$ correspondingly.

From Fig.4 (right panel) we can conclude that the binary mass ratio in SS433 should not be significantly larger than $q \sim 0.3 - 0.35$, because in that case the optical star would be too small to provide the observed depth of the eclipse or the radius of the star (i.e. the radius of the X-ray eclipser which can exceed the actual star radius) should be larger than $R/a \gtrsim 0.5 - 0.55$.

5. Conclusion

Using extensive observational data obtained by RXTE, we studied systematic variations of X-ray emission of SS433 caused by precessional and orbital motions in the system.

We compared X-ray spectra of SS433 near and in the eclipse and obtained strong signatures of a significant ($N_H > 10^{23} \text{ cm}^{-2}$) photoabsorption of X-rays near the companion star. We argue that this may be due to the presence of a dense stellar wind from the companion star. The size of the X-ray eclipsing region can be significantly larger than the size of the Roche lobe due to absorption in the inner stellar wind.

We recovered the temperature profile of plasma along the jet and estimated the jet cross section at its basement. The maximum visible temperature is found to be $T \sim 30 \text{ keV}$ at a distance of $l/a = 0.06 - 0.09$ from the compact object. The radius of the jet at this distance is $r_0/a = 0.01 - 0.016$.

We reliably detected orbital eclipses in the RXTE/PCA observations of SS433 during the “crossover” precessional phases when the X-ray jets and the axis of the accretion disk lie exactly in the plane of the sky. The observed depth of the X-ray eclipse implies that the size of the star is larger than $R/a \gtrsim 0.5$, yielding an upper bound on the mass ratio of the components in SS433 $q < 0.3 - 0.35$ assuming that the radius of the eclipser (star plus inner wind) can not be much larger than $1.2R_{\text{Roche,secondary}}$.

6. Acknowledgements

Research has made use of data obtained from High Energy Astrophysics Science Archive Research Center Online Service, provided by the NASA/Goddard Space Flight Center. This work has been supported by RFBR grants N 04-02-16349, N 05-02-19710, N 06-02-16025, N 04-02-17276 and N 04-02-16720, and by joint RFBR/JSPS grant N 05-02-12710.

References

- Achmad, L., Lemers H.J.G.L.M., & Pasquini, L. 1997, A&A, 320, 196
Fabrika, S. 2004, Astrophysics and Space Physics Reviews, 12, 1
Koval', E. & Shakura N., 1989, in Proc. 23rd ESLAB Symp. on Two-Topics in X-ray Astronomy (ESA SP-296), 479
Marshall, H., Canizares, C., & Schulz, N. 2002, ApJ, 564, 941
Paczynski B., 1977, ApJ, 216, 822